Methanol Synthesis

International Edition: DOI: 10.1002/anie.201600943
German Edition: DOI: 10.1002/ange.201600943

Indium Oxide as a Superior Catalyst for Methanol Synthesis by CO_2 Hydrogenation

*Oliver Martin, Antonio J. Martín, Cecilia Mondelli, Sharon Mitchell, Takuya F. Segawa, Roland Hauert, Charlotte Drouilly, Daniel Curulla-Ferré, and Javier Pérez-Ramírez**

Abstract: *Methanol synthesis by CO_2 hydrogenation is attractive in view of avoiding the environmental implications associated with the production of the traditional syngas feedstock and mitigating global warming. However, there still is a lack of efficient catalysts for such alternative processes. Herein, we unveil the high activity, 100 % selectivity, and remarkable stability for 1000 h on stream of In_2O_3 supported on ZrO_2 under industrially relevant conditions. This strongly contrasts to the benchmark Cu-ZnO-Al_2O_3 catalyst, which is unselective and experiences rapid deactivation. In-depth characterization of the In_2O_3-based materials points towards a mechanism rooted in the creation and annihilation of oxygen vacancies as active sites, whose amount can be modulated in situ by co-feeding CO and boosted through electronic interactions with the zirconia carrier. These results constitute a promising basis for the design of a prospective technology for sustainable methanol production.*

Methanol is a key building block in the chemical industry,[1] with prospects as a sustainable energy carrier if its production is accomplished from CO_2 (captured from large-point emitters) and H_2 (retrieved from renewable sources).[2] This application demands novel catalysts as the ternary Cu-ZnO-Al_2O_3 system currently employed for methanol synthesis from mixed syngas ($CO/CO_2/H_2$) exhibits limited activity in CO_2 hydrogenation, because of the inhibiting effect of the water byproduct,[3] low selectivity, owing to its significant activity in the parasitic reverse water–gas shift (RWGS) reaction,[4] and insufficient stability, due to water-induced sintering of the active phase.[5] Furthermore, the intricate network of synergistic structural and electronic effects between its components hampers the rational optimization of this material.[4a,6] Among other catalysts studied,[7] only Cu-ZnO-Ga_2O_3/SiO_2 and $LaCr_{0.5}Cu_{0.5}O_3$ displayed improved methanol formation rates and high selectivities (up to 99.5 %), but their scalability and long-term stability have not been assessed. Recent experiments on $Cu/CeO_x/TiO_2$ model surfaces[8] also showed promising results, but no attempt has been made to translate this material into a practically relevant polycrystalline solid.

In our quest for a suitable catalyst, we were intrigued by the much simpler In_2O_3 system. This reducible oxide is commonly used together with SnO_2 as a very stable conductive transparent layer in organic light-emitting diodes and thin-film transistors.[9] Moreover, it has demonstrated high activity and selectivity in multiple catalytic transformations involving CO_2, including electrochemical conversion into formic acid,[10] photocatalytic reduction to CO,[11] and methanol steam reforming.[12] Recently, density functional theory (DFT) studies on CO_2 hydrogenation over non-defective[13] and defective[14] $In_2O_3(110)$ surfaces suggested that methanol is the most favorable product and that the reaction follows a mechanism comprising the cyclic creation and annihilation of oxygen vacancies. Analysis by impedance and infrared spectroscopy has revealed an increased conductivity for In_2O_3 that has been exposed to H_2 at mild temperatures,[15] suggesting that vacancies can be present at conditions relevant to methanol synthesis. Subsequent testing of a commercial In_2O_3 sample in CO_2 hydrogenation showed reaction rates comparable to those of Cu-ZnO systems but only moderate methanol selectivities (up to 55 %),[16] in contrast to the DFT predictions.[14] Based on these premises, we synthesized bulk In_2O_3 in a controlled manner and showed that its selectivity to the C_1 alcohol can be tuned up to 100 % under a wide range of industrially relevant conditions ($T = 473$–573 K, $P = 1.0$–5.0 MPa, and gas hourly space velocity (GHSV) $= 16\,000$–$48\,000$ h^{-1}). Moreover, we showed that its activity can be boosted either through CO co-feeding and/or the use of a ZrO_2 support, which interacts strongly with the active phase, without lowering the selectivity. This was correlated with an increase in oxygen vacancies as characterized by spectroscopic and temperature-programmed sorption methods. In_2O_3/ZrO_2 exhibited excellent stability in a 1000 h run and could be prepared in an equivalently performing technical shape, hence paving the way for the development of a new technology for sustainable methanol production.

We assessed the CO_2 hydrogenation performance of self-prepared nanosized In_2O_3 (11 nm, Table 1) versus the benchmark Cu-ZnO-Al_2O_3 catalyst under typical methanol syn-

[*] O. Martin, Dr. A. J. Martín, Dr. C. Mondelli, Dr. S. Mitchell, Prof. J. Pérez-Ramírez
ETH Zurich, Department of Chemistry and Applied Biosciences
Institute for Chemical and Bioengineering
Vladimir-Prelog-Weg 1, 8093 Zurich (Switzerland)
E-mail: jpr@chem.ethz.ch
Dr. T. F. Segawa
ETH Zurich, Department of Chemistry and Applied Biosciences
Laboratory of Physical Chemistry
Vladimir-Prelog-Weg 2, 8093 Zurich (Switzerland)
Dr. R. Hauert
Empa, Swiss Federal Laboratories for Materials Science and Technology
Überlandstrasse 129, 8600 Dübendorf (Switzerland)
Dr. C. Drouilly, Dr. D. Curulla-Ferré
Total Research & Technology Feluy
Zone Industrielle Feluy C, 7181 Seneffe (Belgium)

Supporting information for this article can be found under: http://dx.doi.org/10.1002/anie.201600943.

 © 2016 Wiley-VCH Verlag GmbH & Co. KGaA, Weinheim

Table 1: Characterization data for selected catalysts.

Sample		S_{BET} [$m^2 g_{cat}^{-1}$]	$d_{crystallite}$[a] [nm]	O_{defect}[b] [%]
In_2O_3	Ar	113	11	23
In_2O_3	A[c]	38	17	16
In_2O_3	B[c]	33	16	24
ZrO_2	fresh	110	–	11
In_2O_3/ZrO_2	4 h on stream	82	8	15
In_2O_3/ZrO_2	1000 h on stream	84	10	14

[a] Determined from the (222) reflection of In_2O_3 in the XRD patterns. [b] The fraction of surface oxygen atoms adjacent to a defect was calculated from the deconvoluted O 1s XPS signal (for a detailed description, see Figure S2 in the Supporting Information). [c] These labels refer to the points shown in Figure 1 b.

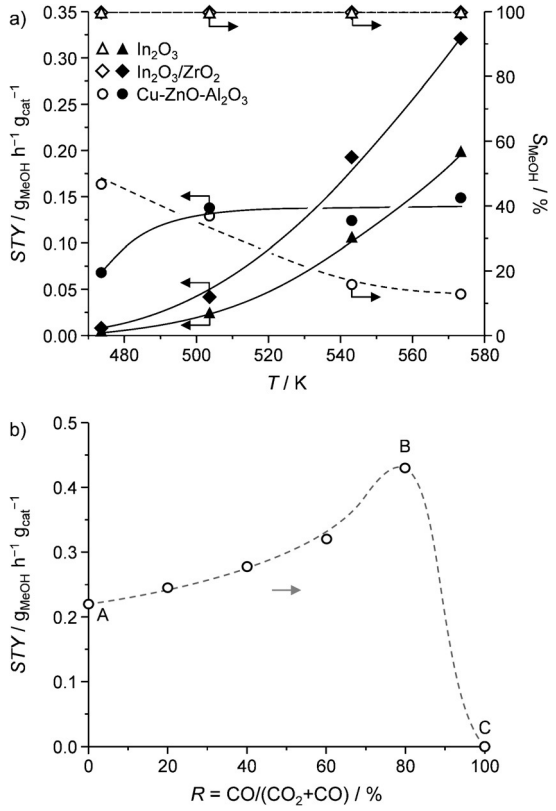

Figure 1. a) Methanol STY and selectivity for CO_2 hydrogenation over bulk In_2O_3, In_2O_3/ZrO_2 (9 wt.% In), and the benchmark Cu-ZnO-Al_2O_3 catalyst at various temperatures. b) Methanol STY over bulk In_2O_3 as a function of the CO concentration in the feed at 573 K. Reaction conditions: $P = 5.0$ MPa, $H_2/CO_2 = 4{:}1$, and GHSV = 16000 h^{-1}.

thesis conditions (Figure 1 a). In_2O_3 showed 100% selectivity to methanol at all temperatures tested, whereas the ternary catalyst only reached a maximum of 47% at 473 K owing to the dominance of the concurrent RWGS reaction.[4a,17] In fact, the selectivity in CO_2 hydrogenation can be tuned by adjusting the GHSV to higher values, at which the slower RWGS vanishes. For In_2O_3, this occurs at GHSV > 16000 h^{-1} (see the Supporting Information, Figure S1a), whereas for Cu catalysts, very high space velocities (6×10^5 h^{-1})[18] are usually required, leading to low single pass conversions. The space time yield (STY) over In_2O_3 is highly temperature-sensitive and greatly exceeds that of the copper catalyst above 560 K. Importantly, In_2O_3 is only moderately affected by H_2O inhibition, as evidenced by the small drop (20%) in reaction rate in a H_2O co-feeding CO_2 hydrogenation experiment at 573 K (molar ratio of $H_2O/CO_2/H_2 = 0.3{:}1{:}4$). In contrast, a 70% decrease in reaction rate has been reported for Cu-ZnO-Al_2O_3 even at 503 K and much larger GHSV values.[18] These results curtail the performance of the Cu-based material at conversion levels relevant for industrial applications.[4a]

Further experiments at the standard reaction temperature of 573 K revealed a linear increase of the STY upon elevating the pressure (1.0–5.0 MPa, Figure S1 b) and a beneficial impact for an excess of hydrogen up to a molar feed ratio of $H_2/CO_2 = 8{:}1$, after which the reaction rate remained constant (Figure S1 c). As no metallic In was detected by powder X-ray diffraction (XRD) after the reaction (Figure 2 a, pattern A), the latter result supports the hypothesis that oxygen vacancies on the indium oxide are the active sites for this reaction. To verify this idea,[14] we studied the reducibility of In_2O_3 by temperature-programmed reduction in hydrogen (H_2-TPR). The reduction feature observed at 373–673 K, prior to the onset of the bulk reduction (Figure 2 b), is in agreement with the existence of such vacancies at the reaction temperatures applied. Subsequently, the In_2O_3 surface was investigated by temperature-programmed desorption (TPD) of CO_2 (Figure 2 d). As oxygen-defective In_2O_3 can be created through thermal treatment or exposure to reducing agents,[14,15] we pretreated the samples either in Ar (at $T = 573$ K) or in diluted H_2 (at $T = 473$ K). Aside from a peak at approximately 360 K, which was attributed to physisorbed CO_2 based on the analysis of a fully oxidized sample (labeled as O_2), two additional signals with maxima at approximately 650 and 590 K were observed; these were assigned to vacancies that are thermally induced (O_{v1}) or formed by H_2 (O_{v2}), respectively.[14]

X-ray photoelectron spectroscopy (XPS) of In_2O_3 pretreated in Ar evidenced a component in the O 1s region related to oxygen atoms next to a defect[11] (O_{defect}, 23%, Table 1; see also Figure S2 a, 531.7 eV). The similar but less intense feature for an oxidized sample (19%) supports the presence of oxygen vacancies as well as other types of defects, such as sub-coordinated In atoms. The surface nature of the defects is corroborated by the disappearance of the O_{defect} signal upon Ar^+ sputtering (Figure S2 b). After use in CO_2 hydrogenation at 573 K, a lower amount of oxygen defects (16%) was determined (Table 1, A), which is in line with the substantial drop in the surface area and the noticeable sintering of the In_2O_3 particles (Table 1 and Figure S3). The latter is induced by H_2 as indicated by the significantly decreased surface area (25 $m^2 g_{cat}^{-1}$) after the treatment of fresh In_2O_3 in pure H_2 at 573 K for one hour. The CO_2-TPD profile of the catalyst after the reaction (Figure 2 d) confirmed contributions from O_{v1} and O_{v2}, and hence, both types of vacancies could participate in the process. Nevertheless, additional catalytic experiments point to the predominant role of thermally induced O_{v1} vacancies: 1) In_2O_3 pretreated in Ar yielded higher STY values than In_2O_3 activated in H_2

 © 2016 Wiley-VCH Verlag GmbH & Co. KGaA, Weinheim

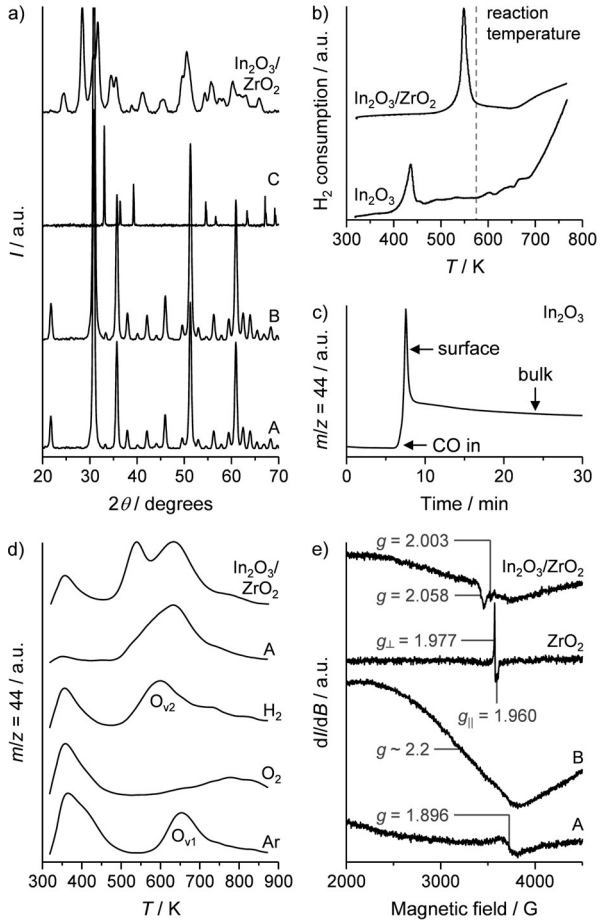

Figure 2. a) XRD patterns, b) H_2-TPR profiles, c) CO_2 evolution upon treatment in diluted CO at 573 K, d) CO_2-TPD curves, and e) EPR spectra for In_2O_3 after different treatments (Ar, O_2, H_2; A, B, and C refer to the points depicted in Figure 1b), the fresh ZrO_2 carrier, and/or the supported catalyst after CO_2 hydrogenation. The XRD patterns of samples A and B exhibit reflections of In_2O_3 only. The latter is completely transformed into metallic In upon exposure to CO/H_2 (C). The pure ZrO_2 carrier did not show any CO_2 adsorption in the CO_2-TPD experiment. The observed EPR signals were assigned to conduction-band electrons ($g = 1.896$), Zr^{3+} centers ($g_\parallel = 1.960$ and $g_\perp = 1.977$), F centers with trapped single electrons ($g = 2.003$), and other unpaired electrons ($g = 2.058$ and ≈ 2.2).

(Figure S4a), and 2) In_2O_3 calcined at higher temperatures (723 vs. 573 K) featured a higher density of active sites, as its activity increased (Figure S4a) in spite of the reduced surface area (Figure S4b). This was further supported by operando diffuse reflectance infrared Fourier transform spectroscopy (DRIFTS), which evidenced bands in agreement with adsorbed CO_2 bridging two In atoms around the O_{v1} site and hydrogenated intermediates formed thereof and did not contain signals specific to carbonate species, which would form upon CO_2 activation over O_{v2} sites (Figure S5). These findings are in agreement with the DFT results by Ge et al.[14] Interestingly, the DRIFTS analysis also revealed the presence of adsorbed CO species whereas no CO was detected at the outlet of the cell, corroborating the slow kinetics of the RWGS reaction under the applied conditions. This undesired pathway becomes only relevant at lower space velocities[16] (Figure S1a) or at higher temperatures and lower H_2 pressures[19] than those used in our study. Therefore, the proper adjustment of the reaction conditions is pivotal to achieving high space time yields and selectivities at reasonable conversion levels over In_2O_3.

Based on its strongly reducing properties, CO was co-fed in the CO_2/H_2 mixture as a strategy to generate vacancies in situ. Indeed, treatment of In_2O_3 in diluted CO at 573 K unveiled a fast reduction of the surface at the beginning of this analysis (Figure 2c). XPS characterization of a sample extracted after 10 min evidenced an improved O_{defect} signal (31%) with respect to the catalyst activated in Ar (23%). The stepwise addition of CO to the gas feed from $R = CO/(CO_2 + CO) = 0$ (point A) to 80% (point B) at 573 K doubled the STY (Figure 1b). The O_{defect} fraction in In_2O_3 substantially increased from A to B (Table 1), which is in line with the performance trend described. Furthermore, electron paramagnetic resonance (EPR; Figure 2e) spectroscopy revealed a single signal at $g = 1.896$ for In_2O_3 used in CO_2 hydrogenation (A), which is related to delocalized electrons populating the conduction band that result from the abstraction of O atoms.[20,21] The additional, broader, and stronger signal at $g \approx 2.2$ for the sample exposed to the CO-rich feed (B) may correlate with another type of vacancy involving unpaired electrons. The relatively low intensity of the EPR signals reflects the surface character of the vacancies, which is in accordance with the XPS results. Both techniques corroborate the role of CO as a vacancy generator and booster of the CO_2 hydrogenation activity to counterbalance the efficient annihilation of vacancies in the presence of CO_2, as indicated by the very stable STY at $R = 0$–80%. Only at $R = 100\%$ (CO/H_2), the reaction rate progressively dropped to 0 within 4 h (point C). No methanol was produced under these conditions also over a fresh catalyst. In line with the decaying CO_2 signal in the CO treatment (Figure 2c) assigned to the steady reduction of the bulk, XRD analysis revealed that CO reduced In_2O_3 to metallic In in the absence of CO_2 (Figure 2a). This phase thus appears to be unable to catalyze CO_2 hydrogenation. As the catalyst remained inactive after switching the syngas composition back to $R = 0\%$, metallic In cannot be reoxidized by CO_2.

Aiming at developing a technically relevant catalyst based on this promising active phase, In_2O_3 was supported (9 wt.% In) onto various carriers to achieve 1) higher dispersion, 2) better resistance against sintering, and possibly also 3) beneficial interactions with the supporting material. Based on the methanol STY and the In-based reaction rate in a CO_2 hydrogenation experiment (Figure 3a), the use of ZrO_2 was advantageous compared to that of other carriers, leading to a material that outperformed bulk In_2O_3 at any reaction temperature (Figure 1a). Evaluation of ZrO_2-supported catalysts with lower or higher In loadings showed that 9 wt.% In is the optimum for the STY, while the reaction rate per gram of In increases with a decreased loading (Figure S6). HRTEM analysis (Figure 3c) visualized intimately mixed crystals of cubic In_2O_3 and monoclinic ZrO_2 in the optimized sample. XRD indicated a smaller particle size for supported In_2O_3 with respect to the bulk catalyst (Table 1). As the latter holds also in the case of the poorly performing In_2O_3/Al_2O_3

 © 2016 Wiley-VCH Verlag GmbH & Co. KGaA, Weinheim

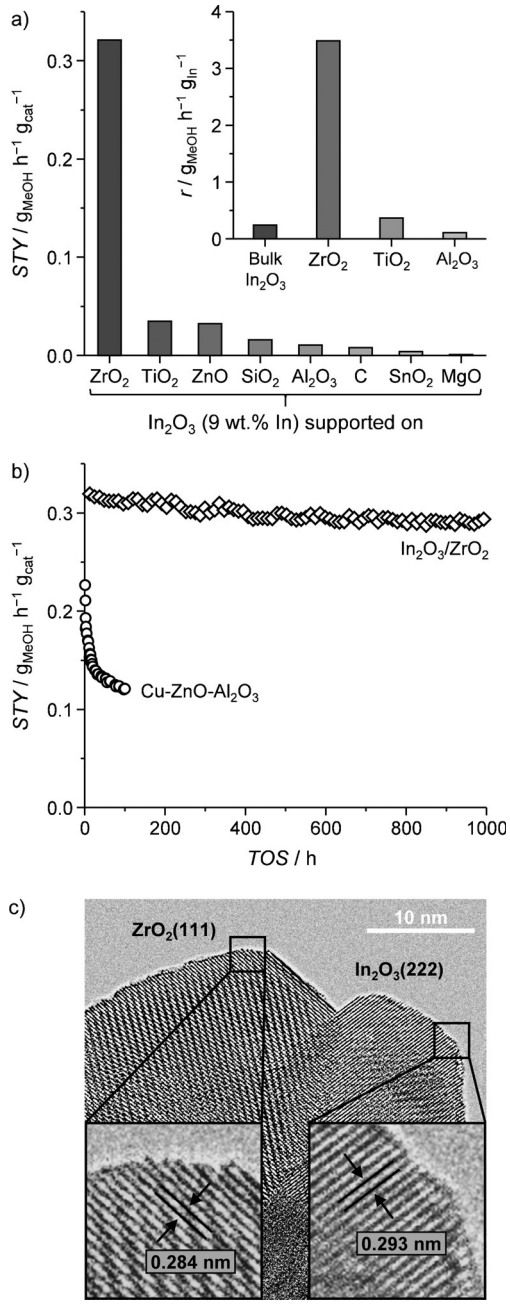

Figure 3. a) Methanol STY for different supported catalysts after 4 h on stream. b) Evolution of the methanol STY with time on stream (TOS) over In_2O_3/ZrO_2 and Cu-ZnO-Al_2O_3. c) HRTEM micrograph of the In_2O_3/ZrO_2 catalyst obtained after 4 h on stream. Reaction conditions: $T = 573$ K, $P = 5.0$ MPa, $H_2/CO_2 = 4{:}1$, and GHSV = 16000 h^{-1}.

(Table S4), the catalytic properties of supported In_2O_3 seem to be determined by electronic interactions with the carrier rather than by geometric effects. This is substantiated by the equally good performance of a material prepared with cubic instead of monoclinic zirconia and by the formation of inactive metallic In in fresh samples with other carriers (Figure S7). The former finding also suggests that the interface between In_2O_3 and the support might be irrelevant for CO_2 activation.

Remarkably, XPS analysis of In_2O_3/ZrO_2 after CO_2 hydrogenation indicated an increase in the O_{defect} signal (Table 1). In fact, its area was larger than the sum of the individual contributions from the carrier and the active phase. Additional insights were given by EPR spectroscopy. At least one type of vacancy was found in the fresh support ($g_{\|} = 1.960$ and $g_{\perp} = 1.977$, Figure 2e), which is related to electrons located in the vicinity of zirconium cations changing their oxidation state from $+4$ to $+3$.[22] These electrons were depleted upon deposition of In_2O_3, suggesting that the reduced Zr centers abstract O atoms from the active phase, thereby creating more and/or new kinds of vacancies. In fact, the EPR spectrum of the supported catalyst contains the same features as those found for bulk In_2O_3 samples used in CO_2 hydrogenation without (A) and with (B) CO co-feeding, as well as two additional signals at $g = 2.003$ and 2.058; the first one was assigned to vacancies with single trapped electrons in ZrO_2 (F centers).[22] Although ZrO_2 itself exhibits no activity for CO_2 hydrogenation under the conditions applied, it cannot be excluded that the vacancies contained in this carrier might also be involved in the reaction mechanism over the supported catalyst.

Aside from this electronic promotion, the ZrO_2 carrier also plays an essential role in preventing the sintering of the In_2O_3 phase, as demonstrated by the excellent stability of In_2O_3/ZrO_2 over 1000 h on stream (Figure 3b). This long-term test was carried out in CO-free syngas to expose the catalyst to the maximum amount of H_2O. The selectivity remained unaltered at 99.8% throughout the experiment, and the activity was only reduced by 8% within the first 400 h on stream, after which the reaction rate was constant. Likewise, the In_2O_3 crystallite size and the catalyst surface area remained unchanged (Table 1). This excellent performance was also observed for a technical In_2O_3/ZrO_2 catalyst obtained by impregnation of extrudates of the carrier. In striking contrast, the conventional Cu-ZnO-Al_2O_3 catalyst underwent substantial loss of activity (44% in 100 h, Figure 3b), which is due to sintering of the Cu and ZnO phases (Figure S8). A comparison of the performance of In_2O_3/ZrO_2 with alternative materials studied in the literature is presented in Table S5.

In conclusion, In_2O_3 has emerged as a highly efficient catalytic system for the hydrogenation of CO_2 to methanol featuring 100% selectivity and outstanding activity under industrially relevant conditions. By confirming the creation of oxygen vacancies by thermal desorption and their annihilation as the key mechanism during the catalytic cycle, we devised strategies at the process and catalyst level to boost its performance. Accordingly, we were able to increase the amount of active vacancies by adding CO to the gas feed or using the electronically interacting ZrO_2 as a carrier for In_2O_3. Remarkably, the supported In_2O_3/ZrO_2 catalyst was stable for 1000 h on stream and could be scaled up to a technical form showing analogous catalytic properties. Hence, we have gained fundamental and applied understanding that paves the way for the exploitation of this novel catalytic system in other processes beyond methanol synthesis.

 © 2016 Wiley-VCH Verlag GmbH & Co. KGaA, Weinheim

Experimental Section

Bulk In_2O_3 was prepared by calcination (573 K, 3 h, static air) of $In(OH)_3$, which had been precipitated by the addition of excess NH_4OH to $In(NO_3)_3{\cdot}x\,H_2O$ dissolved in a 1:3 mixture of deionized water and ethanol. Supported In_2O_3 catalysts (9 wt.% In) in powder or extrudate forms were prepared by impregnation of the carriers with an $In(NO_3)_3{\cdot}x\,H_2O$ solution followed by evaporation of the solvent, drying, and calcination as for bulk In_2O_3. Cu-ZnO-Al_2O_3 was obtained by conventional coprecipitation of hydroxycarbonates. The compositional, textural, and structural properties of the In_2O_3-based catalysts were studied by X-ray fluorescence spectroscopy, N_2 sorption at 77 K, powder X-ray diffraction, and high-resolution transmission electron microscopy, whereas the oxygen vacancies were investigated by temperature-programmed reduction with H_2 or CO, temperature-programmed desorption of CO_2, X-ray photoelectron spectroscopy, and electron paramagnetic resonance spectroscopy. CO_2 hydrogenation was conducted over undiluted catalysts in a fixed-bed reactor setup. Prior to the reaction, the In_2O_3 catalysts were activated in Ar at 573 K and 0.5 MPa for 1 h, whereas the Cu-ZnO-Al_2O_3 catalyst was pretreated in 5 vol.% H_2/Ar under the same conditions. Operando diffuse reflectance Fourier transform infrared spectroscopy was applied to investigate the surface species generated upon CO_2 adsorption and hydrogenation. Further details on catalyst preparation, characterization, and testing are given in the Supporting Information.

Acknowledgements

We thank Total Research & Technology Feluy for sponsoring this research and the Scientific Center for Optical and Electron Microscopy at the ETH Zurich, ScopeM, for the use of their facilities. T.F.S. is grateful to Prof. G. Jeschke for valuable comments on the interpretation of the EPR data.

Keywords: CO_2 hydrogenation · indium oxide · methanol synthesis · oxygen vacancies · zirconium oxide

How to cite: *Angew. Chem. Int. Ed.* **2016**, *55*, 6261 – 6265
Angew. Chem. **2016**, *128*, 6369 – 6373

[1] a) E. Fiedler, G. Grossmann, D. B. Kersebohm, G. Weiss, C. Witte in *Ullmann's Encyclopedia of Industrial Chemistry*, *Vol. 23*, 7th ed., Wiley-VCH, Weinheim, **2012**, pp. 25 – 48; b) E. V. Kondratenko, G. Mul, J. Baltrusaitis, G. O. Larrazábal, J. Pérez-Ramírez, *Energy Environ. Sci.* **2013**, *6*, 3112 – 3135.

[2] G. A. Olah, A. Goeppert, G. K. S. Prakash, *Beyond Oil and Gas: The Methanol Economy*, 2nd ed., Wiley-VCH, Weinheim, **2009**.

[3] F. Studt, M. Behrens, E. L. Kunkes, N. Thomas, S. Zander, A. Tarasov, J. Schumann, E. Frei, J. B. Varley, F. Abild-Pedersen, J. K. Nørskov, R. Schlögl, *ChemCatChem* **2015**, *7*, 1105 – 1111.

[4] a) J. Nakamura, Y. Choi, T. Fujitani, *Top. Catal.* **2003**, *22*, 277 – 285; b) E. L. Kunkes, F. Studt, F. Abild-Pedersen, R. Schlögl, M. Behrens, *J. Catal.* **2015**, *328*, 43 – 48.

[5] M. B. Fichtl, D. Schlereth, N. Jacobsen, I. Kasatkin, J. Schumann, M. Behrens, R. Schlögl, O. Hinrichsen, *Appl. Catal. A* **2015**, *502*, 262 – 270.

[6] a) S. Polarz, J. Strunk, V. Ischenko, M. W. E. van den Berg, O. Hinrichsen, M. Muhler, M. Driess, *Angew. Chem. Int. Ed.* **2006**, *45*, 2965 – 2969; *Angew. Chem.* **2006**, *118*, 3031 – 3035; b) L. Martínez-Suárez, N. Siemer, J. Frenzel, D. Marx, *ACS Catal.* **2015**, *5*, 4201 – 4218; c) J. Schumann, M. Eichelbaum, T. Lunkenbein, N. Thomas, M. C. Álvarez Galván, R. Schlögl, M. Behrens, *ACS Catal.* **2015**, *5*, 3260 – 3270.

[7] W. Wang, S. Wang, X. Ma, J. Gong, *Chem. Soc. Rev.* **2011**, *40*, 3703 – 3727.

[8] J. Graciani, K. Mudiyanselage, F. Xu, A. E. Baber, J. Evans, S. D. Senanayake, D. J. Stacchiola, P. Liu, J. Hrbek, J. F. Sanz, J. A. Rodriguez, *Science* **2014**, *345*, 546 – 550.

[9] A. Kumar, C. Zhou, *ACS Nano* **2010**, *4*, 11 – 14.

[10] Z. M. Detweiler, J. L. White, S. L. Bernasek, A. B. Bocarsly, *Langmuir* **2014**, *30*, 7593 – 7600.

[11] L. B. Hoch, T. E. Wood, P. G. O'Brien, K. Liao, L. M. Reyes, C. A. Mims, G. A. Ozin, *Adv. Sci.* **2014**, *1*, 1400013.

[12] a) N. Iwasa, T. Mayanagi, N. Ogawa, K. Sakata, N. Takezawa, *Catal. Lett.* **1998**, *54*, 119 – 123; b) H. Lorenz, W. Jochum, B. Klötzer, M. Stöger-Pollach, S. Schwarz, K. Pfaller, S. Penner, *Appl. Catal. A* **2008**, *347*, 34 – 42.

[13] J. Ye, C. Liu, Q. Ge, *J. Phys. Chem. C* **2012**, *116*, 7817 – 7825.

[14] J. Ye, C. Liu, D. Mei, Q. Ge, *ACS Catal.* **2013**, *3*, 1296 – 1306.

[15] a) T. Bielz, H. Lorenz, W. Jochum, R. Kaindl, F. Klauser, B. Klötzer, S. Penner, *J. Phys. Chem. C* **2010**, *114*, 9022 – 9029; b) T. Bielz, H. Lorenz, P. Amann, B. Klötzer, S. Penner, *J. Phys. Chem. C* **2011**, *115*, 6622 – 6628.

[16] J. K. Sun, Z. Fan, J. Ye, J. Yan, Q. Ge, Y. Li, W. He, W. Yang, C.-J. Liu, *J. CO_2 Util.* **2015**, *12*, 1 – 6.

[17] J. Yoshihara, C. T. Campbell, *J. Catal.* **1996**, *161*, 776 – 782.

[18] O. Martin, C. Mondelli, D. Curulla-Ferré, C. Drouilly, R. Hauert, J. Pérez-Ramírez, *ACS Catal.* **2015**, *5*, 5607 – 5616.

[19] W. Wang, Y. Zhang, Z. Wang, J. Yan, Q. Ge, C. Liu, *Catal. Today* **2016**, *259*, 402 – 408.

[20] N. Siedl, P. Gügel, O. Diwald, *J. Phys. Chem. C* **2013**, *117*, 20722 – 20729.

[21] W. M. Walsh, J. P. Remeika, L. W. Rupp, *Phys. Rev.* **1966**, *152*, 223 – 228.

[22] H. Liu, L. Feng, X. Zhang, Q. Xue, *J. Phys. Chem.* **1995**, *99*, 332 – 334.

Received: January 27, 2016
Revised: February 21, 2016
Published online: March 17, 2016

 © 2016 Wiley-VCH Verlag GmbH & Co. KGaA, Weinheim